Discrimination Between Eccentricity and Interturn Faults Using Current or Voltage-Reference Signature Analysis in Symmetrical Six-Phase Induction Machines

Alejandro G. Yepes, *Senior Member, IEEE*, Davide S. B. Fonseca, *Member, IEEE*, Hugo R. P. Antunes, Oscar López, *Senior Member, IEEE*, Antonio J. Marques Cardoso, *Senior Member, IEEE*, and Jesús Doval-Gandoy, *Member, IEEE*

***Abstract*—Two common defects in induction machines (IMs) are eccentricity and interturn faults, which should be diagnosed to prevent performance degradation and further damage. A popular fault-detection approach is the current signature analysis (CSA), because of its simplicity and nonintrusiveness. Under closed-loop control, it is combined with analogous voltage-reference (VR) signature analysis (VRSA). However, by using these methods in three-phase IMs, it is difficult to discriminate between these faults, which cause similar symptoms. Multiphase machines provide remarkable advantages such as inherent tolerance to open-phase faults. Six-phase IMs are particularly attractive since they allow adopting three-phase converters. Among them, those with symmetrical spatial arrangement of the stator phases offer superior fault tolerance. Nonetheless, the distinction between eccentricity and interturn failures in these IMs has not been addressed so far. This article studies the discrimination between eccentricity and interturn faults in symmetrical six-phase (S6) IMs by CSA or VRSA. It is shown that, conversely to three-phase IMs and most other multiphase IMs, in S6 ones, these two types of failures can be easily distinguished: interturn faults considerably alter the currents or VRs in the so-called x-y plane, whereas eccentricity leads to current/voltage symptoms only in the α_1-β_1 plane. Experimental results confirm the theory.**

Manuscript received 25 April 2022; revised 2 August 2022; accepted 8 September 2022. Date of publication 12 September 2022; date of current version 18 November 2022. This work was supported in part by the European Regional Development Fund (ERDF) through the Operational Programme for Competitiveness and Internationalization (COMPETE 2020) under Project POCI-01-0145-FEDER-029494, in part by National Funds through the FCT - Portuguese Foundation for Science and Technology under Projects PTDC/EEI-EEE/29494/2017, UIDB/04131/2020, UIDP/04131/2020, and UI/BD/153572/2022, in part by the Government of Galicia under the Grants ED431F 2020/07 and GPC-ED431B 2020/03, in part by the Ministry of Science, Innovation and Universities under the Ramon y Cajal Grant RYC2018-024407-I, and in part by the Spanish State Research Agency (AEI) under Project PID2019-105612RB-I00/AEI/10.13039/501100011033. Recommended for publication by Associate Editor M. Su. *(Corresponding author: Jesús Doval-Gandoy.)*

Alejandro G. Yepes, Oscar López, and Jesús Doval-Gandoy are with the Applied Power Electronics Technology (APET) Research Group, CINTECX, Universidade de Vigo, 36310 Vigo, Spain (e-mail: agyepes@uvigo.es; olopez@uvigo.es; jdoval@uvigo.es).

Davide S. B. Fonseca, Hugo R. P. Antunes, and Antonio J. Marques Cardoso are with the CISE - Electromechatronic Systems Research Centre, University of Beira Interior, 6201-001 Covilhã, Portugal (e-mail: davide.fonseca@ieee.org; hugo.antunes@ubi.pt; ajmcardoso@ieee.org).

Color versions of one or more figures in this article are available at https://doi.org/10.1109/TPEL.2022.3206141.

Digital Object Identifier 10.1109/TPEL.2022.3206141

***Index Terms*—Condition monitoring, eccentricity, fault diagnosis, interturn faults, multiphase machines, six-phase machines.**

I. Introduction

SHORT-CIRCUIT failures between different turns of the stator winding, i.e., interturn faults, are one of the most usual faults in electric machines [1], [2], [3]. This problem is normally caused by aging of the insulation [2], as a result of thermal, electrical, mechanical, and environmental stress during the machine operating life [1], [4]. Another common defect in electric machines is rotor eccentricity [5], which means that the airgap length is not uniform [1]. This occurs when the rotor geometrical axis (static eccentricity) or rotation axis (dynamic eccentricity) is displaced with respect to its ideal location, i.e., the stator axis of symmetry [1], [6]. In most cases, both static and dynamic eccentricity arise simultaneously, a phenomenon known as mixed eccentricity [1], [6], [7]. A certain degree of mixed eccentricity is unavoidable due to manufacturing tolerances [1], [8], [9], but it can be aggravated by, e.g., shaft misalignment and bearing defects [1], [6].

It is important to properly diagnose eccentricity and interturn faults, to apply accordingly the most appropriate corrective measures. These actions can be fixing the defective machine part or, in some cases, adequately reconfiguring the control (for eccentricity [10] or interturn [11], [12], [13], [14], [15], [16], [17], [18] faults) or drive topology (for interturn failures [19], [20], [21]) for the meantime. Otherwise, the drive performance is degraded (e.g., by efficiency reduction and torque ripple) and further damage can be produced (e.g., stator-rotor rub or supply/ground faults) [1], [2], [6], [8]. Arguably, the most popular approach for fault diagnosis is based on the stator current signature analysis (CSA) because of its simplicity and nonintrusiveness [2], [22]. In ac drives with closed-loop control, although the current harmonics may be attenuated to some extent by the control, analogous symptoms arise then in the voltage references (VRs), and, hence, CSA can be combined with analogous VR signature analysis (VRSA) [5], [6], [23]. In principle, CSA and VRSA do not need injection of extra signals

TABLE I
CLASSIFICATION OF REFERENCES ABOUT DETECTION OF ECCENTRICITY OR INTERTURN FAULTS IN MULTIPHASE MACHINES

References	Machine			Detection		Signal injection	Monitored signals	Extra* sensors
	n	Windings	Rotor	Eccentricity	Interturn			
Andriamalala et al. [6]	**6**	**Sym.**	**IM**	Yes	No	No	d_1-q_1 or phase current or VR	No
Choi et al. [9]	5	Sym.	PMaSynRM	Yes	No	No	d_1-q_1 current	No
Pazouki et al. [42]	5	Sym.	PMaSynRM	Yes	No	No	Phase back-EMF	No
Torres et al. [43]	5	Sym.	PMaSynRM	Yes	No	No	Phase current and ZS voltage	No
Maouche et al. [44]	6	Asym.	IM	Yes	No	No	ZS voltage	Yes
Wang et al. [45]	**6**	**Sym.**	**IM**	Yes	No	High frequency	ZS current and VR	No
Silva et al. [47]	6	Asym., 0-ph.	IM	No	Yes	No	x-y current	No
Andriamalala et al. [46]	6	Asym., 0-ph.	IM	No	Yes	No	Phase current	No
Foito et al. [48]	**6**	**Sym.**	**IM**	No	Yes	No	x-y current	No
Immovili et al. [49]	5	Sym.	PMSM	No	Yes	No	α_1-β_1 & x-y current or voltage	No
Sundaram et al. [50]	5	Sym.	IM	No	Yes	dc	Phase current and VR	No
Gritli et al. [23]	6	Asym.	PMSM	No	Yes	No	x-y current or VR	No
Amirouche et al. [53]	6	Asym.	PMSM	No	Yes	No	ZS voltage and phase currents	Yes
Abad et al. [51], [52]	6	Asym.	IM	No	Yes	No	x-y current	No
Wu et al. [13]	6	Sym.	PMSM	No	Yes	High frequency	Phase current and VR	No
Antunes et al. [3]	**6**	**Sym.**	**IM**	No	Yes	No	Phase current and voltage	No
This article	**6**	**Sym.**	**IM**	Yes	Yes	No	α_1-β_1 & x-y current or VR	No

* Besides usual stator-current sensors. If the extra sensors are optional, "No" is indicated.

or installation of additional sensors. However, by using these methods in star-connected three-phase machines, it is difficult to discriminate between eccentricity and interturn faults because they give rise to similar current (or VR) symptoms [1], [24]. This limitation is related to the fact that, when the model of a three-phase machine is analyzed by the vector space decomposition (VSD), there is only one stator plane (α_1-β_1) where current can flow. The VSD permits to associate each space harmonic with certain stator orthogonal subspaces, but for three phases, all current-producing space harmonics are mapped into the α_1-β_1 plane, regardless of whether they are related to healthy operation, eccentricity, interturn faults, or other conditions [25]. Moreover, the orders of the space harmonics affected by eccentricity and interturn faults, although many, usually match for both types of problems [1], [24]. For instance, a change in the magnitude of the negative-sequence α_1-β_1 fundamental current (or ellipticity of α_1-β_1 current trajectory) is often employed to detect either eccentricity [5] or interturn [1], [26], [27], [28], [29] faults, without CSA/VRSA-based distinction between them. Actually, it is suggested in [5] to add voltage measurement of the zero-sequence (ZS) in order to discriminate both possible causes of this symptom, at the expense of extra sensors. Similarly, the magnitude of rotor slot harmonics (RSHs) in the current can be altered by either eccentricity [1], [24], [30], [31], [32] or interturn [24], [30] faults, making it difficult to distinguish both faults by these symptoms as well [1], [30], [32]. In any case, most of the existing studies in this regard are focused on three-phase machines.

On the other hand, multiphase (n-phase) machines are being the focus of increasing attention due to significant advantages concerning aspects such as enhanced fault tolerance, low torque pulsation, and reduced current rating for given power [33], [34], [35], [36]. Six-phase machines are particularly attractive since they allow adopting off-the-shelf three-phase converter modules [34], [37]. Among six-phase induction machines (IMs), those with symmetrical spatial arrangement of the stator phases offer especially large achievable torque and low losses under open- or short-circuit phase faults [38], [39], [40] as well as high dc-link utilization and control simplicity with reduced x-y undesired currents in healthy operation [41]. Given the potential of multiphase machines, several authors have addressed the detection of eccentricity [6], [9], [42], [43], [44], [45] or interturn [3], [13], [23], [46], [47], [48], [49], [50], [51], [52], [53] faults in them (summarized in Table I), with a few of these publications being focused on symmetrical six-phase (S6) IMs (bold in Table I) [3], [6], [45], [48].

Andriamala et al. [6] propose to detect mixed eccentricity in an S6 IM with two isolated neutral points by monitoring the RSHs in a per-phase current (or VR) or in the d_1-q_1 rotating frame within the α_1-β_1 plane. The sensitivity of the x-y currents to eccentricity is not discussed. Choi et al. [9] define a fault index for eccentricity that adequately combines the current signals of all phases, analogously to a projection onto a d_1-q_1 frame. It is shown that the robustness to noise is greater than by monitoring a single phase current. This technique is tested in a five-phase permanent magnet assisted synchronous reluctance motor (PMaSynRM) [9], whose fault symptoms are different from IMs. For other five-phase PMaSynRMs, eccentricity is detected by means of the harmonics in the back electromotive force (back EMF) [42] or phase voltage/currents [43]. Maouche et al. [44] suggest to add a voltage sensor between the neutral points of an asymmetrical six-phase (A6) IM to detect the ZS eccentricity symptoms. Wang et al. [45] diagnose either static or dynamic eccentricity in an S6 IM by injecting a high-frequency signal into the *ZS*-axis, but the IM is required to have a single neutral point instead of two, and the injected signal increases the losses, as well as the peak phase voltage and current.

Concerning interturn faults, Silva et al. [47] monitor the x-y current of a six-phase IM for their detection, but no results are presented for symmetrical winding layout, just for asymmetrical and no-phase-shift (0-ph.) arrangements. In [46], it is shown that the frequencies of the interturn and broken-bar symptoms in an A6 IM are similar to three-phase IMs when monitoring a phase current. Foito et al. [48] diagnose interturn faults in an S6 IM with separate neutral points, assuming that the x-y current trajectory is a single point in healthy situation and a circle in case

of failure. In particular, the radius of this x-y circle is measured for the detection. However, in practice, the x-y current under interturn fault may contain several frequencies, describing a non-circular trajectory. Immovili et al. [49] detect interturn faults in a five-phase permanent-magnet synchronous machine (PMSM), by monitoring the dc and second-order harmonics of the product between α_1-β_1 and x-y vectors of either current or voltage. These harmonics result from the combination of positive- and negative-sequence fundamental components in both planes. It is claimed that this fault index is robust to eccentricity [49], but this property is only checked by simulations for a specific five-phase PMSM with certain winding layout and pole pairs, not in general for any machine. Sundaram et al. [50] inject a dc signal to measure the dc resistance of each phase of a five-phase IM, although it implies (as in [45]) certain losses and increase of the peak phase current and voltage. Gritli et al. [23] monitor the amplitude of the positive and negative sequences of the fundamental and third-harmonic x-y currents or VRs in an A6 PMSM. For the same type of machine, Amirouche et al. [53] propose to diagnose interturn faults by integrating a certain expression as a function of the ZS voltage and the per-phase currents, based on the PMSM model. For an A6 IM, Abad et al. [51], [52] show that interturn faults are reflected as an elliptical trajectory in the x-y plane, and they define a fault index based on the largest diameter [51] or on its difference with respect to the smallest [52]. A high-frequency signal is injected into the synchronous d_1-axis of an S6 PMSM in [13], with similar shortcomings as the aforesaid ones regarding the eccentricity diagnosis method from [45]. Antunes et al. [3] derive a per-phase machine model of an S6 IM, but the VSD components are not exploited for fault diagnosis.

From the preceding literature survey and Table I, several main conclusions can be drawn. Although there are various papers about detection of eccentricity or interturn faults in multiphase machines, only a few of them address eccentricity [6], [45] or interturn [3], [48] faults in S6 IMs, in spite of the interest of this kind of machine [38], [40], [41]. Most importantly, the distinction between eccentricity and interturn failures by means of CSA/VRSA in S6 IMs has not been addressed yet. It is commonly acknowledged that it is difficult in general (regardless of the machine) to distinguish the symptoms of these two types of faults when using just CSA/VRSA [1], [24], but no indication that S6 IMs could be advantageous in this regard has been shown or hinted so far.

This article addresses the distinction of eccentricity and interturn faults in S6 IMs by CSA or VRSA, as reflected in the last row of Table I. It is shown in this article that, conversely to three-phase IMs, in S6 ones, these two types of failures can be easily distinguished: interturn faults produce considerable variation of the x-y stator current (or VR), whereas eccentricity leads to current (or VR) symptoms only in the α_1-β_1 plane (analogous to three-phase IMs). This behavior also differs from other multiphase machines such as A6 IMs, where both kinds of problems result in x-y current (or VR) changes making the distinction more difficult. The diagnosis can be thus performed in S6 IMs without adding voltage sensors or injecting additional signals.

The article is organized as follows. The theoretical analysis is presented in Section II, the laboratory setups in Section III, and the experimental results in Section IV.

II. Theoretical Analysis

The fundamentals of the VSD are reviewed in Section II-A, the current symptoms of eccentricity are discussed in Section II-B, and those of interturn faults in Section II-C. The effect of closed-loop control is here neglected initially, since its addition would only mean that, if some of the current symptoms are attenuated, analogous symptoms arise in the VRs [5], [6], [23]. Finally, some remarks about the effects of other disturbances and faults are briefly discussed in Section II-D. Although the focus of this article is on S6 IMs, the theory is initially presented in general for different types of windings in order to highlight the advantages of such particular case.

A. Vector Space Decomposition (VSD)

The VSD decomposes the stator variables into several subspaces that are, in principle, orthogonal to each other [25], [39]. For an n-phase machine, the VSD can be applied to a vector of stator per-phase signals as follows [25], [39]:

$$\begin{bmatrix} u_{\alpha_\sigma \mathrm{s}} \\ u_{\beta_\sigma \mathrm{s}} \end{bmatrix} = \frac{2}{n} \begin{bmatrix} \cos(\sigma\phi_\mathrm{a}) & \cos(\sigma\phi_\mathrm{b}) & \cdots & \cos(\sigma\phi_n) \\ \sin(\sigma\phi_\mathrm{a}) & \sin(\sigma\phi_\mathrm{b}) & \cdots & \sin(\sigma\phi_n) \end{bmatrix} \begin{bmatrix} u_{\mathrm{as}} \\ \vdots \\ u_{n\mathrm{s}} \end{bmatrix} \tag{1}$$

where σ denotes a subspace, ϕ is the spatial angle of each stator phase, and u_s may be current, voltage, or flux linkage in the stator. In a given subspace, u_s can be expressed as a complex vector $\underline{u}_{\alpha\beta_\sigma \mathrm{s}} = u_{\alpha_\sigma \mathrm{s}} + \mathrm{j}u_{\beta_\sigma \mathrm{s}}$.

The most common types of stator winding arrangements are symmetrical (consecutive phases displaced by $2\pi/n$) and asymmetrical (three-phase sets displaced by π/n) [25], [33], [35], [39], [41], [54]. The following σ values exist: $\sigma = 0, 1, 2, \ldots, \lfloor n/2 \rfloor$ for symmetrical windings and $\sigma = 1, 3, 5, \ldots, 2\lceil n/2 \rceil - 1$ for asymmetrical [25], [39]. The so-called *ZS*-axes correspond to $\sigma = n/2$ (if n is even) and $\sigma = 0$ (always) for symmetrical windings, and to $\sigma = n/2$ (if n is even) or $\sigma = n$ (if n is odd) for asymmetrical [25], [39]. For the ZSs σ such that one of the rows in (1) is null, the remaining row should be divided by 2. The subspaces other than α_1-β_1 and ZSs are often called x-y planes, as done henceforth in this article. For instance, in an S6 IM, there is an α_1-β_1 plane ($\sigma = 1$), an x-y plane ($\sigma = 2$), and two *ZS*-axes ($\sigma = 0, 3$, referred to as 0^+ and 0^-). In an A6 IM, the σ values change for the x-y plane ($\sigma = 5$) and *ZS*-axes ($\sigma = 3$).

B. VSD Current Symptoms of Eccentricity

In the absence of interturn faults, a space harmonic of order ν linked by the stator is mapped into stator subspace σ according to [25], [54]

$$\nu = \sigma \pm \lambda^\mathrm{s} n \tag{2}$$

where $\lambda^\mathrm{s} = 0, 1, 2, \ldots$ or $\lambda^\mathrm{s} = 0, 2, 4, \ldots$ for symmetrical or asymmetrical windings, respectively. The sign of ν reflects

whether the corresponding space vector rotates clockwise or counterclockwise within its subspace σ.

Neglecting saturation and rotor current harmonics, the flux space harmonics linked by the stator can be produced by the rotor/stator slotting and eccentricity:

$$\nu = \lambda^{\mathrm{sr}} + \frac{1}{p}\left(\lambda^{\mathrm{qr}} Q_{\mathrm{r}} + \lambda^{\mathrm{qs}} Q_{\mathrm{s}} + \lambda^{\mathrm{se}} + \lambda^{\mathrm{de}}\right). \tag{3}$$

In this expression, Q_{r} and Q_{s} represent the number of rotor and stator slots, respectively, and p is the number of pole pairs. The variables λ^{qr}, λ^{qs}, λ^{se}, and λ^{de} can be any integers. The se and de supercripts refer to static and dynamic eccentricity, respectively. The variable λ^{sr} may be $+1$ or -1, so that the ν signs in (2) and (3) are consistent [25]. Equation (3) is obtained by combining the expressions in [25] (ignoring eccentricity) and [7] (ignoring ν sign). A space harmonic ν generated according to (3) produces noticeable induced voltage in the stator if the magnitude of the νth harmonic is significant in the stator winding function; in such a case, this component is mapped into a stator subspace σ obeying (2). The induced voltage harmonic causes a change (often increase) in the stator current in the same subspace and with the same time frequency as this voltage, unless the impedance for σ is infinite (e.g., *ZS*-axes for isolated neutral points). Based on [7] and [25], the current/voltage time frequency associated with a certain ν can be computed by substituting the corresponding values of the parameters from (3) into

$$\omega_{\mathrm{h}} = \omega_{\mathrm{s}}\left[\lambda^{\mathrm{sr}} + \frac{(1-s_{\mathrm{l}})}{p}\left(\lambda^{\mathrm{qr}} Q_{\mathrm{r}} + \lambda^{\mathrm{de}}\right)\right] \tag{4}$$

with ω_{s} being the α_1-β_1 stator fundamental frequency and s_{l} the slip. Thus, eccentricity can be diagnosed by detecting a current component of frequency ω_{h} in a subspace σ given by (2) such that it corresponds with $\lambda^{\mathrm{se}} \neq 0$ or $\lambda^{\mathrm{de}} \neq 0$ in (3).

In IMs with odd n or with asymmetrical windings of even n, all stator subspaces are affected by odd space harmonics [see (2)], which can be produced by eccentricity [see (3)]. For instance, an A6 IM contains odd space harmonics $\nu = 1, -11, 13, \ldots$ and $\nu = 5, -7, 17, -19, \ldots$ in the α_1-β_1 ($\sigma = 1$) and x-y ($\sigma = 5$) planes, respectively [see (2)]. Thus, when eccentricity is present, associated current components of various frequencies arise in both stator planes. For example, fundamental x-y current may exist due to eccentricity.

In contrast, based on (2), the stator x-y plane ($\sigma = 2$) of an S6 IM only contains even harmonics ($\nu = 2, -4, 8, \ldots$). The magnitude of these even harmonics can be disregarded, because the space harmonics in the stator winding of an IM are usually just of odd integer orders. It also follows from (2) that the harmonic orders mapped into the α_1-β_1 plane ($\sigma = 1$) are the same for three-phase and S6 machines ($\nu = 1, -5, 7, -11, 13, \ldots$). That is, eccentricity can be detected in an S6 IM by using CSA as for a three-phase IM. This is, in fact, done in [6], but the distinction from interturn faults or the absence of x-y eccentricity symptoms was not discussed.

C. VSD Current Symptoms of Interturn Faults

The VSD model of an S6 IM under interturn fault is given in the Appendix. It is obtained by following an analogous mathematical derivation to that presented in [55] for three-phase IMs. Based on the model in the Appendix, it follows that in an S6 IM, the x-y stator current due to an interturn fault (disregarding x-y supply excitation: $\underline{v}_{xy\mathrm{s}} = 0$) is

$$\underline{i}_{xy\mathrm{s}} = \underline{i}_{\alpha\beta_2\mathrm{s}} = i_{x\mathrm{s}} + \mathrm{j} i_{y\mathrm{s}} = \frac{1}{3}\mu \mathrm{e}^{\mathrm{j}\gamma} i_{\mathrm{f}} \tag{5}$$

where μ is the ratio of shorted turns over total turns of a phase, i_{f} is the fault current through the short-circuit path, and

$$\gamma = -k\frac{2\pi}{n} \tag{6}$$

where k denotes the faulty phase as 0 for phase a, 1 for b, 2 for c, etc. Note that i_{f} is mainly (neglecting harmonics) a sinusoidal signal of frequency ω_{s}. Although machine models for S6 IMs in this situation can be found in previous papers [3], [47], explicit closed-form expressions of the x-y current under fault [as in (5)] were not provided.

The fact that there is current induced in the x-y plane seems to be in contradiction with the equation for mapping of space harmonics into VSD subspaces, i.e., (2). This is because (2) relies on the assumption that the stator winding distribution is identical for all phases. This hypothesis still holds true in case of eccentricity, because such problem alters the spatial harmonic content of the airgap flux, not the stator windings [7]. On the contrary, an interturn fault implies a change in the electrical circuits within the windings of one phase [3], [55]. In effect, the winding of the affected phase ceases to behave as those of other stator phases. Thus, the voltage induced in this phase by the flux linkage becomes different. Accordingly, the induced voltage is no longer balanced across all phases, even if the airgap flux distribution is balanced. As a consequence, any space harmonic ν (e.g., $\nu = 1$) is no longer mapped into a single stator subspace according to (2) but is instead mapped into various subspaces [including x-y, as in (5)] simultaneously.

In most types of multiphase IMs, interturn failures could be misdiagnosed because of x-y symptoms of eccentricity, analogously to three-phase IMs, where similar current symptoms of both problems arise in the same plane (in that case, α_1-β_1) [1], [24]. On the other hand, in an S6 IM, although x-y current is expected to arise due to interturn failures according to (5), eccentricity does not produce x-y current, as justified in Section II-B. Hence, it follows that the amount of x-y current can be employed to distinguish between eccentricity and interturn faults in this kind of IM.

D. Effects of Other Disturbances and Faults

It should be remarked that the symptoms under study do not coincide with low-order disturbances introduced by converter nonlinearities, which normally arise at integer harmonic orders mapped according to (2) (replacing ν by time harmonic order) [56], [57], [58]. Open-circuit faults in the inverter or machine, which are out of the scope of this article, can also cause considerable x-y current, but they may be distinguished by checking, e.g., if a phase current is null [59]. Regarding switch short-circuits, most switch drivers are able to detect them [60],

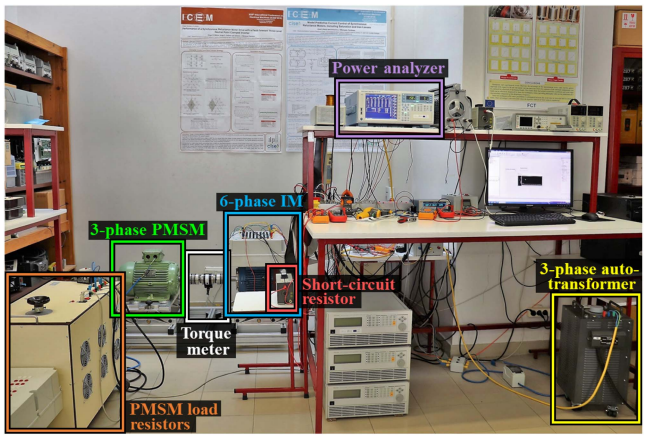

(a)

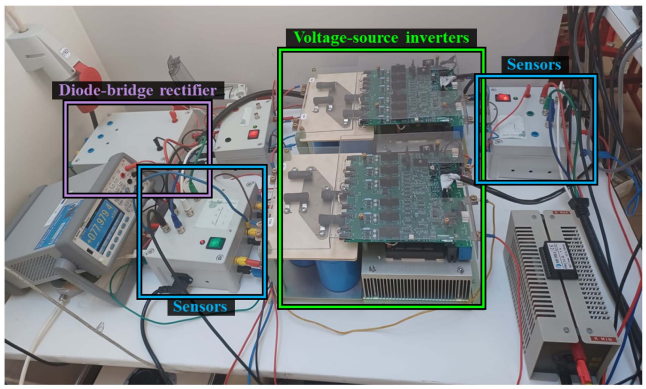

(b)

Fig. 1. Experimental setup of S6 IM. (a) Global view. (b) Power electronics.

(a) (b) (c)

Fig. 2. Mechanism to introduce eccentricity in S6 IM, according to [64]. (a) Outer ring, in an end cap. (b) Inner ring. (c) Both rings, mounted onto each other.

[61], e.g., by monitoring the ON-state voltage drop [62]. Broken bars may be distinguished from eccentricity by checking whether the average torque decreases, which typically occurs for the former [63].

III. Experimental Setups

Two laboratory setups are employed, one with an S6 IM (Section III-A) and another one with an A6 IM (Section III-B). Since this paper is focused on S6 IMs, the attention is mainly devoted to the former, with extensive tests of eccentricity and interturn faults. Eccentricity results with the A6 IM are only used to show more clearly the advantage of S6 IMs over other ones such as A6 IMs, thanks to the fact that in S6 IMs eccentricity does not cause x-y symptoms, unlike in A6 ones.

A. Setup for S6 IM

A four-pole S6 IM has been prepared for testing eccentricity and interturn faults in the laboratory setup shown in Fig. 1. This S6 IM was obtained by rewinding a Dahlander dual-speed three-phase IM, which had power and speed ratings of 6 kW and 2930 r/min for two-pole configuration and of 1.5 kW and 1460 r/min for four-pole configuration, with rated phase voltage of 230 V and rated current per coil of 5.7 A. The rewinding was done so that the S6 IM has the same rated current per coil (5.7 A per phase), while the phase voltage was derated to 150 V. A stator phase was set so that tappings at different points of its winding are available for applying short circuits, while limiting the resulting current by an external 2-Ω resistor R_{f} in parallel with the shorted turns [3]. The eccentricity is introduced by a mechanism similarly to [64]. Namely, each bearing housing of the motor was replaced by a pair of eccentric rings mounted onto each other (see Fig. 2), so that the amount of eccentricity is modified by adjusting the relative position between these rings. Although, theoretically, this only produces static eccentricity, it is known that, in practice, dynamic eccentricity commonly arises with it as a by-product [7]. The percentages of eccentricity given subsequently are of the static type. Other important parameters of the S6 IM are $p = 2$, $Q_{\mathrm{r}} = 28$, and $Q_{\mathrm{s}} = 36$. Further details about this IM can be found in [3].

As shown in Fig. 1(a), the S6 IM is coupled to a three-phase PMSM, whose stator is connected to a three-phase resistor load. The torque is measured by a Magtrol TMB-310/411 torque meter. In some of the tests, the IM is driven in open loop with rated stator frequency ($f_{\mathrm{s}} = 50$ Hz), by connecting the two three-phase sets of the IM to each other in antiparallel and to the grid through a three-phase autotransformer, while the data acquisition is performed by a Yokogawa WT1800 power analyzer. A single neutral point is set so that the symptoms in the ZS current $i_{0\text{-}\mathrm{s}}$ can be studied. Tests at other electrical frequencies or with closed-loop control are instead carried out by feeding the S6 IM using a pair of three-phase Powerex POW-R-PAK inverters [see Fig. 1(b)] switching at 5 kHz and controlled by a dSPACE DS1103. The dc-link voltage is kept at 374 V by the grid through the autotransformer and a diode-bridge rectifier. When using the converter, the two stator neutral points are isolated to avoid ZS high-frequency circulating currents due to the switching. For closed-loop control, indirect rotor field-oriented control with proportional–integral speed and current regulators is adopted in the α-β plane. The converter modulation is designed so that only the so-called large α-β voltage vectors are selected, preventing high-frequency x-y disturbances and the need for x-y closed-loop control [41].

B. Setup for A6 IM

A few tests are also done with an A6 IM with ratings of 18.5 kW, 16 A, 230 V, and 1470 r/min. For this IM, $p = 2$, $Q_{\mathrm{r}} = 44$, and $Q_{\mathrm{s}} = 48$. Static eccentricity is introduced by replacing the normal end plates by ones with a displacement equal to 30% of the airgap. The motor is driven in open-loop by a six-phase converter based on insulated-gate bipolar transistors

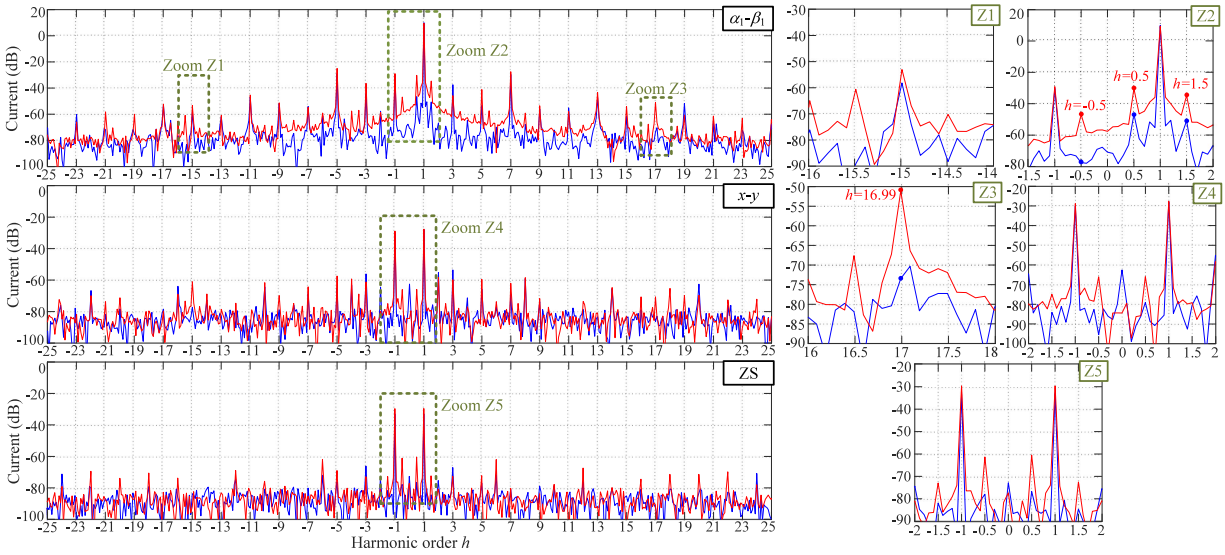

Fig. 3. Experimental VSD current spectrum of S6 IM at 0-Nm load and $f_s = 50$ Hz, in healthy condition (blue) and with 65% eccentricity (red).

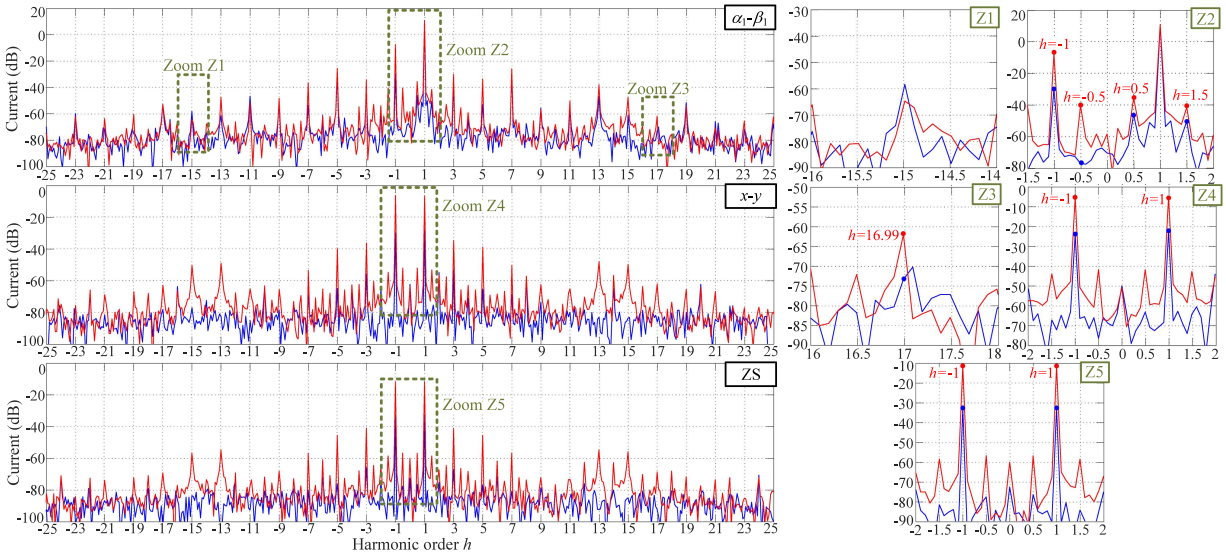

Fig. 4. Experimental VSD current spectrum of S6 IM at 0-Nm load and $f_s = 50$ Hz, in healthy condition (blue) and with 23 shorted turns (red).

and switching at 10 kHz. The control and signal acquisition are performed by a dSPACE-MicroLabBox platform. The load torque is applied by a 12-phase PMSM [65], [66], with resistors connected to its stator.

IV. Experimental Results

The results for the S6 IM (most important) are presented in Section IV-A. Those obtained with the A6 IM are briefly discussed in Section IV-B, for the sake of completeness.

A. Experiments With S6 IM

The tests with the S6 IM fed by the grid ($f_s = 50$ Hz) are discussed first. For each interturn/eccentricity scenario, three conditions of load torque are tested: 0 (no load), 10, and 16 Nm, for which the speeds are 1499, 1471, and 1452 r/min, respectively. The resulting VSD current spectrum is shown in Figs. 3 and 4 for 0-Nm load and in Figs. 5 and 6 for 16-Nm load. Figs. 3 and 5 display in red the results for 65% eccentricity,

TABLE II
Integer Variables Corresponding to the Experimental Current Harmonics of S6 IM Due to Eccentricity

h ($f_s = 50$ Hz)			h ($f_s = 25$ Hz)		ν	λ^{qr}	λ^{qs}	λ^{se}	λ^{de}	λ^{sr}	σ
0 Nm	10 Nm	16 Nm	0 Nm	10 Nm							
−14.99	−14.69	−14.49	−14.98	−13.87	−17	−1	0	−4	−4	1	1
−1.00	−1.00	−1.00	−1.00	−1.00	1	0	0	4	0	−1	1
−0.50	−0.47	−0.45	−0.50	−0.39	1	0	0	3	−3	1	1
0.50	0.51	0.52	0.50	0.54	1	0	0	1	−1	1	1
1.50	1.49	1.48	1.50	1.46	1	0	0	−1	1	1	1
16.99	16.69	16.49	16.98	15.87	19	1	0	4	4	1	1

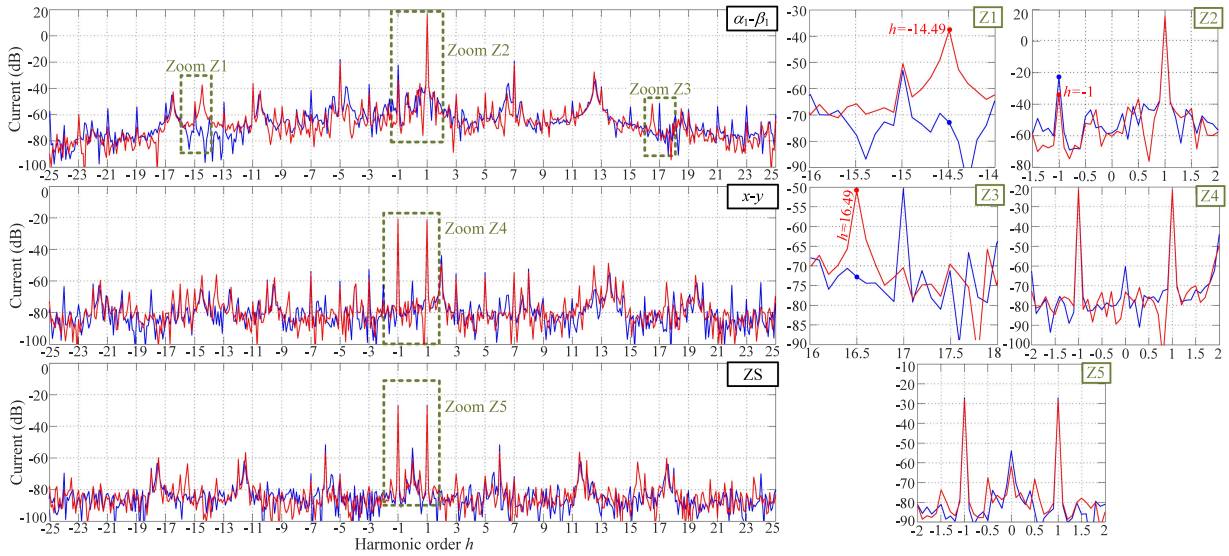

Fig. 5. Experimental VSD current spectrum of S6 IM at 16-Nm load and $f_s = 50$ Hz, in healthy condition (blue) and with 65% eccentricity (red).

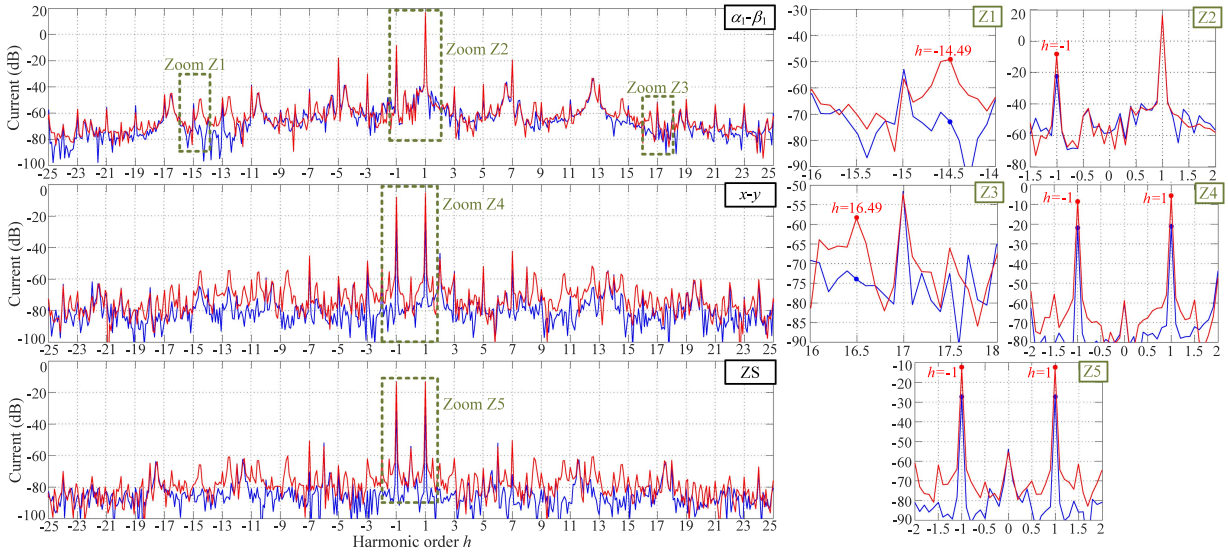

Fig. 6. Experimental VSD current spectrum of S6 IM at 16-Nm load and $f_s = 50$ Hz, in healthy condition (blue) and with 23 shorted turns (red).

whereas Figs. 4 and 6 show in red those for 23 shorted turns (out of 138 turns, in phase a). In each of these figures, the spectrum for the same load but without introducing eccentricity/interturn faults is shown in blue, for comparison.

From Figs. 3–6, when eccentricity or interturn faults are present, noticeable current symptoms arise in the spectrum (red) in comparison with healthy condition (blue). For a given load, the symptoms in the α_1-β_1 plane are similar for both kinds of faults, as expected. Namely, for either fault, the main alterations in the α_1-β_1 current occur at the time harmonic orders $h = -0.5, 0.5, 1.5, 16.99$ for no-load (compare Figs. 3 and 4) and at $h = -14.49, 16.99$ for 16-Nm load (compare Figs. 5 and 6). Although at no-load, the magnitude of the α_1-β_1 current at $h = -1$ is modified with shorted turns and not with eccentricity (see Figs. 3 and 4), this component is not a reliable indicator for discrimination, because at high load, it also changes with eccentricity (see Figs. 5 and 6) and it is, in fact, used to detect eccentricity in other works [5]. Some values of the theoretical integer variables that justify these eccentricity symptoms according to (2)–(4) are given in Table II. For example, it can be checked that the numbers in the first row for 16-Nm load are consistent with (2), (3), and (4):

$$-17 = 1 - 3 \cdot 6 \tag{7}$$

$$-17 = -1 + \frac{1}{2}(1 \cdot 28 + 0 \cdot 36 - 4 - 4) \tag{8}$$

$$-14.49 = 1 + \frac{(1 - s_1)}{2}(-1 \cdot 28 - 4) \tag{9}$$

TABLE III
EXPERIMENTAL MAGNITUDE OF THE MAIN CURRENT COMPONENTS OF S6 IM AT 0-NM LOAD AND $f_s = 50$ Hz

Eccentricity (%)	Shorted turns	α_1-β_1 current (dB)						x-y current (dB)		ZS current (dB)
		$h=-1$	$h=-0.5$	$h=0.5$	$h=1$	$h=1.5$	$h=16.99$	$h=-1$	$h=1$	$h=\pm1$
0	0	−30.12	−77.36	**−46.53**	10.00	**−50.61**	**−70.34**	**−30.00**	**−27.88**	−32.99
20	0	−27.04	−46.84	**−33.93**	9.88	**−42.87**	**−59.44**	−26.71	−26.41	−30.52
35	0	−29.67	−50.07	**−31.80**	9.73	**−37.78**	**−54.79**	−25.64	−24.63	−30.50
50	0	−31.78	−46.03	**−30.79**	9.67	**−35.12**	**−55.07**	−26.97	−26.73	−30.80
65	0	−28.96	−46.86	**−30.23**	9.56	**−34.61**	**−51.09**	−28.85	−27.62	−29.66
0	8	−24.78	−53.39	−41.90	10.01	−61.42	−66.48	**−24.24**	−29.67	−26.93
0	12	−18.33	−46.12	−40.28	10.08	−47.80	−64.64	**−16.90**	**−18.61**	−21.43
0	19	−10.41	−41.84	−36.84	10.31	−44.69	−62.54	**−10.14**	**−10.66**	−15.01
0	23	−7.85	−40.75	−35.90	10.56	−41.83	−62.16	**−6.50**	**−6.58**	−11.78
35	12	−20.26	−42.26	**−31.56**	9.75	**−34.37**	**−61.02**	**−16.19**	**−20.22**	−21.16
65	23	−9.17	−39.29	**−30.60**	10.07	**−32.60**	**−52.36**	**−7.24**	**−7.36**	−12.37

TABLE IV
EXPERIMENTAL MAGNITUDE OF THE MAIN CURRENT COMPONENTS OF S6 IM AT 16-NM LOAD AND $f_s = 50$ Hz

Eccentricity (%)	Shorted turns	α_1-β_1 current (dB)				x-y current (dB)		ZS current (dB)
		$h=-14.49$	$h=-1$	$h=1$	$h=16.49$	$h=-1$	$h=1$	$h=\pm1$
0	0	**−72.92**	−22.68	16.08	−74.06	**−21.63**	**−21.27**	−27.10
20	0	**−66.79**	−26.21	15.85	−66.54	−23.08	−22.24	−28.26
35	0	**−63.87**	−28.51	15.88	−72.30	−22.87	−22.28	−28.75
50	0	**−46.44**	−25.72	15.93	−59.05	−20.48	−21.08	−28.45
65	0	**−37.76**	−34.05	15.83	−52.26	−20.87	−21.43	−28.05
0	8	−64.57	−21.71	16.10	−72.09	**−30.56**	**−16.55**	−26.83
0	12	−59.02	−17.87	16.18	−67.68	−22.93	**−12.80**	−22.67
0	19	−51.25	−11.32	16.42	−63.26	**−12.84**	**−8.31**	−16.43
0	23	−49.25	−8.64	16.64	−58.53	**−8.19**	**−5.51**	−12.90
35	12	**−52.50**	−17.64	16.00	−66.78	−23.42	**−12.93**	−22.90
65	23	**−35.00**	−8.03	16.47	−49.16	**−8.74**	**−5.69**	−12.90

where $s_l = (1500 - 1452)/1500$. Note that the current harmonics due to $\nu = -17$ and $\nu = 19$ could also be obtained with $\lambda^{qs} = \pm 1$ and $\nu = 1$, which may explain why they are especially relevant. Most importantly, the results from Figs. 3–6 confirm that monitoring only the α_1-β_1 current or a single-phase current (as done, e.g., in [6] for the same kind of IM) may not be sufficient in order to distinguish eccentricity and interturn faults.

It can also be observed in Figs. 3 and 5 that eccentricity does not cause any remarkable change in the x-y or ZS current, regardless of the load. For instance, the fundamental component in these subspaces is nearly unaltered. Conversely, Figs. 4 and 6 show that significant current components become present in the x-y and ZS subspaces when the interturn failure is applied, as expected from theory, due to the winding imbalance. In particular, the fundamental current ($h = \pm 1$) increases to a great extent in both subspaces. In any case, the ZS current would not be available if the two stator neutral points were not connected to each other, which is sometimes preferred in order to reduce losses and enhance dc-link utilization [65], [67]. Furthermore, the ZS third-order space harmonic may actually be excited by eccentricity in other IMs, as can be inferred from (2)–(4) and as reported in three-phase IMs [68]. On the other hand, the x-y plane lacks these shortcomings. Therefore, it is verified that the amount of x-y current can be employed to discriminate eccentricity and interturn faults.

The values of the current magnitudes in dB corresponding to the aforesaid symptoms are displayed in Table III for 0-Nm load and in Table IV for 16-Nm load. The data is also included for different degrees of severity, and for the combination of both failure kinds. The results for 10-Nm load are shown in Table V. The most relevant symptoms are indicated in bold. These tables corroborate that the main conclusions drawn from Figs. 3–6 also hold for less severe faults and other loads: the current components altered by either eccentricity or interturn faults are similar in the α_1-β_1 plane, whereas just the latter type of failure gives rise to significant current change in the x-y plane. It can also be seen in Tables III and IV that in most cases, these symptoms tend to rise gradually with the amount of eccentricity and shorted turns, providing an indication of the fault severity. It is also worth noting that in the x-y plane, both the positive- and negative-sequence fundamental components due to interturn faults have considerable magnitudes, i.e., the current trajectory is much closer to elliptical than to circular; thus, previous methods for S6 IMs relying on the assumption of circular x-y trajectory (as in [48]) would not be suitable here. These positive and negative sequences are not identical to each other [as in (5)] because of supply and machine nonidealities, but their magnitude change is sufficient for diagnosis nonetheless.

Concerning the scenario of simultaneous eccentricity and interturn faults (last two rows in Tables III–V), it can be observed

TABLE V
EXPERIMENTAL MAGNITUDE OF THE MAIN CURRENT COMPONENTS OF S6 IM AT 10-NM LOAD AND $f_s = 50$ Hz

Eccentricity (%)	Shorted turns	α_1-β_1 current (dB)				x-y current (dB)		ZS current (dB)
		$h=-14.69$	$h=-1$	$h=1$	$h=16.69$	$h=-1$	$h=1$	$h=\pm1$
0	0	**−71.48**	−26.06	13.30	−71.79	**−21.81**	**−21.34**	−27.10
20	0	**−76.81**	−21.52	15.85	−73.91	−23.61	−23.19	−29.05
35	0	**−66.17**	−26.53	13.25	−70.34	−24.10	−22.28	−29.85
50	0	**−48.98**	−24.36	13.08	−63.59	−23.47	−22.77	−29.45
65	0	**−42.07**	−20.89	13.24	−58.25	−22.31	−21.88	−28.37
0	8	−63.71	−23.66	13.30	−70.74	**−27.57**	**−16.93**	−28.10
0	12	−57.89	−18.76	13.40	−58.43	−21.83	**−13.11**	−23.49
0	19	−53.55	−11.26	13.73	−54.09	**−12.94**	**−8.32**	−16.75
0	23	−52.47	−7.88	13.93	−49.89	**−8.08**	**−5.51**	−12.96
35	12	**−55.77**	−18.61	13.38	−69.02	−22.17	**−13.08**	−23.32
65	23	**−40.58**	−8.33	13.88	−60.66	**−8.45**	**−5.72**	−13.17

TABLE VI
EXPERIMENTAL MAGNITUDE OF THE MAIN CURRENT COMPONENTS OF S6 IM AT 0-NM LOAD AND $f_s = 25$ Hz

Eccentricity	Shorted	α_1-β_1 current (dB)						x-y current (dB)	
0	0	−39.23	**−83.08**	**−45.42**	8.50	−47.90	**−58.02**	**−32.30**	**−35.15**
20	0	−37.68	**−76.73**	−42.07	8.41	−47.18	**−65.80**	−31.41	−34.29
35	0	−41.79	**−59.25**	**−38.63**	8.14	−46.20	**−54.59**	−32.79	−34.40
50	0	−36.92	**−58.18**	**−37.06**	8.18	−41.49	**−46.47**	−32.27	−34.86
65	0	−36.71	**−54.31**	**−36.83**	8.08	−42.01	**−48.16**	−33.91	−36.36
0	8	−34.29	−79.02	−44.25	8.43	−47.06	−49.15	−31.27	**−31.55**
0	12	−25.41	−64.47	−45.36	8.39	−45.00	−44.00	**−29.26**	**−28.46**
0	19	−18.61	−58.53	−46.50	8.41	−43.79	−42.77	**−24.51**	**−24.03**
0	23	−15.31	−53.64	−46.69	8.48	−42.25	−47.14	**−20.84**	**−20.42**
35	12	−25.41	**−59.19**	**−37.50**	8.19	−41.91	−58.92	**−28.89**	**−29.50**
65	23	−15.45	**−50.41**	**−35.88**	8.20	−39.92	**−43.22**	**−20.38**	**−20.96**

TABLE VII
EXPERIMENTAL MAGNITUDE OF THE MAIN CURRENT COMPONENTS OF S6 IM AT 10-NM LOAD AND $f_s = 25$ Hz

Eccentricity (%)	Shorted turns	α_1-β_1 current (dB)				x-y current (dB)	
		$h=-13.87$	$h=-1$	$h=1$	$h=15.87$	$h=-1$	$h=1$
0	0	**−65.42**	−29.70	13.86	−66.83	**−20.38**	**−26.73**
20	0	**−60.57**	−29.66	14.08	−63.44	−23.09	−26.87
35	0	**−50.69**	−30.55	13.81	−60.70	−23.44	−25.97
50	0	**−42.30**	−29.22	13.80	−55.78	−22.31	−25.56
65	0	**−32.25**	−29.36	13.71	−49.53	−22.29	−25.48
0	8	−62.22	−26.56	13.87	−67.68	**−26.52**	−24.76
0	12	−58.23	−22.81	13.90	−66.38	**−34.03**	**−21.95**
0	19	−52.75	−17.72	14.00	−65.58	**−29.75**	**−18.74**
0	23	−53.83	−13.74	14.09	−63.42	−21.55	**−16.14**
35	12	**−50.76**	−22.44	13.88	−64.33	**−32.56**	**−21.44**
65	23	**−40.23**	−14.58	14.17	−55.24	−22.26	**−15.63**

that the symptoms of both failures are combined. Thus, in such a case, it is not obvious whether just the latter exists or both of them do. Since an interturn fault is more critical, this one may be repaired first, and then it can be checked if the α_1-β_1 symptoms remain (eccentricity is present) or not. In this kind of situations, the proposed approach is mainly advantageous in the sense that it permits to know with certainty that an interturn failure has occurred, because the x-y change could not be caused by just eccentricity.

The data displayed in Tables VI and VII are obtained for loads of 0 and 10 Nm (speeds of 749 and 697 r/min), respectively, while supplying the IM by the voltage-source inverter using $f_s =$ 25 Hz and open-loop *Vlf* control. The harmonic orders of the symptoms change in accordance with Table II. From Tables VI and VII, the preceding conclusions drawn for $f_s = 50$ Hz also hold for a lower fundamental frequency. Principally, it can be seen that only the α-β components are affected by eccentricity, whereas the fundamental x-y current is substantially altered by interturn faults. In this case, the symptoms are slightly less clear than for $f_s = 50$ Hz, because of the smaller back EMF, but they are still sensitive enough for the diagnosis.

The preceding results were acquired while feeding the IM in open loop. This kind of control is of interest in many applications, especially because of its simplicity [69]. Nevertheless,

TABLE VIII
EXPERIMENTAL MAGNITUDE OF THE MAIN CURRENT COMPONENTS OF S6 IM AT 0-NM LOAD AND $f_s = 50$ Hz, USING CLOSED-LOOP CONTROL

Eccentricity (%)	Shorted turns	α_1-β_1 current (dB)						x-y current (dB)	
		$h=-1$	$h=-0.5$	$h=0.5$	$h=1$	$h=1.5$	$h=16.99$	$h=-1$	$h=1$
0	0	−52.87	−47.49	−34.29	7.69	−34.42	**−71.03**	**−30.83**	**−32.75**
20	0	−47.45	−47.48	−37.66	7.62	−39.28	**−61.92**	−29.33	−31.42
35	0	−39.98	−49.63	−36.78	7.94	−35.35	**−56.47**	−29.61	−30.97
50	0	−35.45	−42.69	−33.07	7.60	−32.69	**−52.69**	−29.81	−31.21
65	0	−35.97	−40.16	−34.76	8.24	−34.72	**−49.94**	−27.83	−30.66
0	8	−34.33	−47.80	−40.09	8.09	−41.94	−63.37	**−25.98**	**−28.94**
0	12	−32.45	−46.46	−35.74	8.07	−36.65	−56.39	**−21.29**	**−22.05**
0	19	−28.41	−46.30	−34.59	8.35	−35.94	−52.13	**−16.35**	**−15.66**
0	23	−28.29	−55.37	−35.97	8.42	−36.82	−50.59	**−12.99**	**−12.01**
35	12	−30.24	−45.46	−32.29	8.02	−32.08	**−54.57**	**−20.95**	**−21.84**
65	23	−27.84	−56.17	−31.68	8.40	−31.45	**−52.23**	**−13.22**	**−12.33**

TABLE IX
EXPERIMENTAL MAGNITUDE OF THE MAIN VR COMPONENTS OF S6 IM AT 0-NM LOAD AND $f_s = 50$ Hz, USING CLOSED-LOOP CONTROL

Eccentricity (%)	Shorted turns	α_1-β_1 current (dB)						x-y current (dB)	
		$h=-1$	$h=-0.5$	$h=0.5$	$h=1$	$h=1.5$	$h=16.99$	$h=-1$	$h=1$
0	0	−4.73	−10.15	**−2.95**	42.21	−3.97	**−21.47**	–	–
20	0	−7.27	−2.91	**1.98**	41.76	−1.49	**−16.18**	–	–
35	0	6.71	−7.00	**3.34**	41.92	0.34	**−11.50**	–	–
50	0	9.32	−2.66	**5.12**	42.02	−0.51	**−6.42**	–	–
65	0	9.75	3.04	**5.98**	42.37	4.84	**−3.90**	–	–
0	8	12.12	−6.90	−11.69	42.40	−5.72	−15.45	–	–
0	12	14.23	−7.06	−4.57	41.93	−4.31	−12.12	–	–
0	19	18.23	−3.03	−4.29	40.18	−2.02	−3.98	–	–
0	23	18.50	−13.32	−6.93	38.79	−3.70	−4.62	–	–
35	12	15.65	−7.52	2.12	40.99	−3.43	**0.02**	–	–
65	23	18.12	−7.29	−11.80	38.33	−8.24	**2.48**	–	–

the conclusions presented here regarding current symptoms are also suitable for drives controlled in closed loop, where the same components (with equivalent behavior) could be monitored in the VRs as well [5], [6], [23]. To illustrate this fact, the values of the fault symptoms for $f_s = 50$ Hz and no-load in the case of closed-loop field-oriented control are shown in Tables VIII and IX for the current measurements and VRs, respectively. In the α-β plane, the most important current symptom for open-loop operation (see Table III) was that at $h = 16.99$. It can be noted that for closed loop (see Tables VIII and IX), the magnitude of this component increases with either eccentricity or interturn faults in both voltage and current, analogously to the current symptom for open loop (cf., Table III). The α-β symptoms at lower frequencies are more difficult to distinguish in the currents (see Table VIII) because the current controller provides greater attenuation of them [5], but the increasing trend of these symptoms with fault severity can anyway be distinguished in the VRs (see Table IX). Similarly, if a controller with higher gain at $h = 16.99$ were implemented, monitoring the VRs would become much more reliable than CSA. Concerning the x-y plane, since it is not affected by the closed-loop control, the behavior of the symptoms is similar to open loop, i.e., they rise just with shorted turns.

B. Experiments With A6 IM

The A6 IM is driven in open-loop with a fundamental frequency of 45 Hz, loaded so that it runs at 1320 r/min. The current spectrum without (blue) and with (red) 30% eccentricity is shown in Fig. 7, for the same load. There is a noticeable change at $h = -1$ and $h = 1$ in the α_1-β_1 ($\sigma = 1$) and x-y ($\sigma = 5$) planes, respectively. These eccentricity symptoms are in agreement with (2)–(4) by using the values displayed in Table X for the variables in these equations. The magnitudes of these harmonics decrease in Fig. 7 with increasing eccentricity because in healthy condition, there is unavoidable practical imbalance, which is common in these machines [70]. This is not a problem *per se* for diagnosis, because the degree of variation could be tracked. Most importantly, the alteration of the fundamental component in the x-y plane for 30% eccentricity (see zoom Z2 of Fig. 7) is much greater than that obtained in the S6 IM for 65% eccentricity (see zoom Z4 of Figs. 3 and 5), even though the eccentricity was more than twice for the S6 IM. As reflected in Table XI, this change for the A6 IM is of about 8 dB. In fact, the x-y symptom at $h = 1$ is of magnitude similar to the α_1-β_1 one at $h = -1$, which is used for eccentricity diagnosis in other publications, e.g., for three-phase IMs [5]. These results further confirm that

TABLE X
INTEGER VARIABLES CORRESPONDING TO THE EXPERIMENTAL CURRENT HARMONICS OF A6 IM DUE TO ECCENTRICITY

h	ν	λ^{qr}	λ^{qs}	λ^{se}	λ^{de}	λ^{sr}	σ
−1	1	0	0	4	0	−1	1
1	1	0	0	8	0	1	5

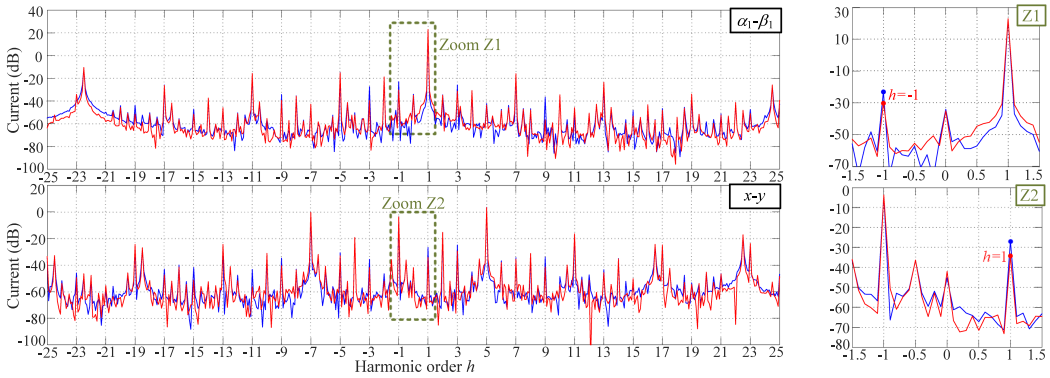

Fig. 7. Experimental VSD current spectrum of A6 IM in healthy condition (blue) and with 30% eccentricity (red).

TABLE XI
EXPERIMENTAL MAGNITUDE OF THE MAIN CURRENT COMPONENTS OF A6 IM

Eccentricity (%)	α_1-β_1 current (dB)		x-y current (dB)	
	$h=-1$	$h=1$	$h=-1$	$h=1$
0	−22.77	22.87	−3.61	**−26.24**
30	−30.42	22.93	−3.61	**−34.66**

in multiphase machines different from S6 IMs, such as A6 ones, it is more likely that x-y current symptoms could arise due to eccentricity and be misdiagnosed as interturn faults.

V. CONCLUSION

This article has addressed the discrimination between eccentricity and interturn faults in S6 IMs by monitoring the stator current or VR signals. It has been shown that, although in most machines, these problems produce similar current or VR symptoms; in this specific kind of IM, it is particularly simple to distinguish them, without signal injection or extra sensors. The key lies in the fact that, in this IM, shorted turns lead to a significant change of the stator current or VR in the x-y plane, whereas neither static nor dynamic eccentricity cause noticeable variation of the x-y current or VR. Accordingly, in spite of the fact that the current or VR symptoms in the α_1-β_1 plane are similar for these faults (as occurs also in three-phase IMs), it can be deduced that a given fault is of interturn type if the x-y current or VR varies substantially. This advantageous feature is not available in other multiphase IMs despite having x-y planes as well, because in most of those machines, the eccentricity symptoms may also be present in x-y. In the majority of multiphase IMs (e.g., A6 ones), numerous space harmonics of odd integer order (susceptible to eccentricity) are always mapped into the stator x-y planes, whereas the x-y plane of an S6 IM is only affected by such harmonics if the structure of the winding is altered, as occurs in an interturn failure.

Possible subjects of future research include the ability to locate the interturn failures within the machine and the discrimination from other faults such as those in the bearings, broken rotor bars, resistance dissymmetry, etc.

APPENDIX

The VSD model of an S6 IM with an interturn fault in a certain phase is given next. It is obtained by following a derivation analogous to that presented in [55] for three-phase IMs. Space harmonics are disregarded. The resulting model is

$$\underline{v}_{\alpha\beta_1\mathrm{s}} = (R_\mathrm{s}+sL_\mathrm{s})\,\underline{i}_{\alpha\beta_1\mathrm{s}} + sL_\mathrm{m}\underline{i}_{\alpha\beta_1\mathrm{r}} - \frac{2}{6}\mu\mathrm{e}^{\mathrm{j}\gamma}\,(R_\mathrm{s}+sL_\mathrm{s})\,i_\mathrm{f} \tag{10}$$

$$\underline{v}_{xy\mathrm{s}} = (R_\mathrm{s}+sL_\mathrm{ls})\,\underline{i}_{xy\mathrm{s}} - \frac{2}{6}\mu\mathrm{e}^{\mathrm{j}\gamma}\,(R_\mathrm{s}+sL_\mathrm{ls})\,i_\mathrm{f} \tag{11}$$

$$v_{0^+\mathrm{s}} = (R_\mathrm{s}+sL_\mathrm{ls})\,i_{0^+\mathrm{s}} - \frac{1}{6}\mu\,(R_\mathrm{s}+sL_\mathrm{ls})\,i_\mathrm{f} \tag{12}$$

$$v_{0^-\mathrm{s}} = (R_\mathrm{s}+sL_\mathrm{ls})\,i_{0^-\mathrm{s}} - \frac{1}{6}\mu\,(R_\mathrm{s}+sL_\mathrm{ls})\,i_\mathrm{f} \tag{13}$$

$$0 = [R_\mathrm{r}+(s-\mathrm{j}\omega_\mathrm{r})\,L_\mathrm{r}]\,\underline{i}_{\alpha\beta_1\mathrm{r}} + (s-\mathrm{j}\omega_\mathrm{r})\,L_\mathrm{m}\underline{i}_{\alpha\beta_1\mathrm{s}} - \frac{2}{6}\,(s-\mathrm{j}\omega_\mathrm{r})\,\mu\mathrm{e}^{\mathrm{j}\gamma}L_\mathrm{m}i_\mathrm{f} \tag{14}$$

where s is the Laplace operator, ω_r is the electrical rotor speed, R_s and R_r are the stator and rotor resistances, L_ls and L_lr are the stator and rotor leakage inductances, L_s and L_r are the stator and rotor self-inductances, and L_m is the magnetizing inductance. The terms introduced by the interturn fault are those affected by the short-circuit current i_f in (10)–(14). The current and voltages in the rotor subspaces other than α_1-β_1 are unaltered by the failure and remain zero. Note that $i_{0^+\mathrm{s}}$ and $i_{0^-\mathrm{s}}$ should be set to zero in this model if there is no ZS current path for them.

The expression corresponding to the short-circuit path is shown in (15), shown at the bottom of this page, with R_f being the equivalent fault resistance in parallel with the shorted turns.

$$R_\mathrm{f}i_\mathrm{f} = \mu R_\mathrm{s}\left(\Re\left\{\mathrm{e}^{-\mathrm{j}\gamma}\underline{i}_{\alpha\beta_1\mathrm{s}}\right\} + \Re\left\{\mathrm{e}^{-\mathrm{j}\gamma}\underline{i}_{xy\mathrm{s}}\right\} + i_{0^+\mathrm{s}} + i_{0^-\mathrm{s}} - i_\mathrm{f}\right) + s\mu L_\mathrm{ls}\left(\Re\left\{\mathrm{e}^{-\mathrm{j}\gamma}\underline{i}_{\alpha\beta_1\mathrm{s}}\right\} + \Re\left\{\mathrm{e}^{-\mathrm{j}\gamma}\underline{i}_{xy\mathrm{s}}\right\} + i_{0^+\mathrm{s}} + i_{0^-\mathrm{s}}\right)$$
$$+ s\mu L_\mathrm{m}\left(\Re\left\{\mathrm{e}^{-\mathrm{j}\gamma}\underline{i}_{\alpha\beta_1\mathrm{s}}\right\} + \Re\left\{\mathrm{e}^{-\mathrm{j}\gamma}\underline{i}_{\alpha\beta_1\mathrm{r}}\right\}\right) - s\mu\left(L_\mathrm{ls} + \frac{2}{6}\mu L_\mathrm{m}\right)i_\mathrm{f}. \tag{15}$$

REFERENCES

[1] S. Nandi, H. A. Toliyat, and X. Li, "Condition monitoring and fault diagnosis of electrical motors–A review," *IEEE Trans. Energy Convers.*, vol. 20, no. 4, pp. 719–729, Dec. 2005.

[2] K. N. Gyftakis and A. J. M. Cardoso, "Reliable detection of stator interturn faults of very low severity level in induction motors," *IEEE Trans. Ind. Electron.*, vol. 68, no. 4, pp. 3475–3484, Apr. 2021.

[3] H. R. P. Antunes, D. S. B. Fonseca, and A. J. M. Cardoso, "Modeling of symmetrical six-phase induction machines under stator faults," in *Proc. IEEE Int. Electric Mach. Drives Conf.*, 2021, pp. 1–7.

[4] A. Siddique, G. S. Yadava, and B. Singh, "A review of stator fault monitoring techniques of induction motors," *IEEE Trans. Energy Convers.*, vol. 20, no. 1, pp. 106–114, Mar. 2005.

[5] L. Wu, X. Huang, T. G. Habetler, and R. G. Harley, "Eliminating load oscillation effects for rotor eccentricity detection in closed-loop drive-connected induction motors," *IEEE Trans. Power Electron.*, vol. 22, no. 4, pp. 1543–1551, Jul. 2007.

[6] R. N. Andriamalala, H. Razik, L. Baghli, and F.-M. Sargos, "Eccentricity fault diagnosis of a dual-stator winding induction machine drive considering the slotting effects," *IEEE Trans. Ind. Electron.*, vol. 55, no. 12, pp. 4238–4251, Dec. 2008.

[7] J. R. Cameron, W. T. Thomson, and A. B. Dow, "Vibration and current monitoring for detecting airgap eccentricity in large induction motors," *Proc. Inst. Elect. Eng.*, vol. 133, no. 3, pp. 155–163, May 1986.

[8] M. Riera-Guasp, J. A. Antonino-Daviu, and G.-A. Capolino, "Advances in electrical machine, power electronic, and drive condition monitoring and fault detection: State of the art," *IEEE Trans. Ind. Electron.*, vol. 62, no. 3, pp. 1746–1759, Mar. 2015.

[9] S. Choi, M. S. Haque, A. Arafat, and H. A. Toliyat, "Detection and estimation of extremely small fault signature by utilizing multiple current sensor signals in electric machines," *IEEE Trans. Ind. Appl.*, vol. 53, no. 3, pp. 2805–2816, May/Jun. 2017.

[10] D. Keller, A. Karayel, H. Naumoski, and N. Parspour, "Influence of static eccentricities on performance and control of dual three-phase permanent magnet synchronous machines," in *Proc. 10th Int. Electric Drives Prod. Conf.*, 2020, pp. 1–8.

[11] A. J. Mitcham, G. Antonopoulos, and J. J. A. Cullen, "Implications of shorted turn faults in bar wound PM machines," *IEE Proc.-Electric Power Appl.*, vol. 151, no. 6, pp. 651–657, Nov. 2004.

[12] P. Arumugam, T. Hamiti, and C. Gerada, "Turn-turn short circuit fault management in permanent magnet machines," *IET Electric Power Appl.*, vol. 9, no. 9, pp. 634–641, Nov. 2015.

[13] F. Wu, A. M. EL-Refaie, and P. Zheng, "Diagnosis and remediation of single-turn short circuit in a multiphase FSCW PM machine based on T-type equivalent circuit," *IEEE Trans. Ind. Appl.*, vol. 56, no. 1, pp. 158–169, Jan./Feb. 2020.

[14] B. Wang, J. Wang, A. Griffo, and L. Huang, "A turn fault mitigation strategy based on current injection technique for a triple three-phase PMA SynRM," *IEEE Trans. Ind. Electron.*, vol. 67, no. 4, pp. 2511–2522, Apr. 2020.

[15] C. Gerada et al., "The results do mesh," *IEEE Ind. Appl. Mag.*, vol. 13, no. 2, pp. 62–72, Mar. 2007.

[16] A. Mohammadpour and L. Parsa, "Global fault-tolerant control technique for multiphase permanent-magnet machines," *IEEE Trans. Ind. Appl.*, vol. 51, no. 1, pp. 178–186, Jan./Feb. 2015.

[17] R. Cui, Y. Fan, and C. Li, "On-line inter-turn short-circuit fault diagnosis and torque ripple minimization control strategy based on OW five-phase BFTHE-IPM," *IEEE Trans. Energy Convers.*, vol. 33, no. 4, pp. 2200–2209, Dec. 2018.

[18] Y. Fan, R. Cui, and A. Zhang, "Torque ripple minimization for inter-turn short-circuit fault based on open-winding five phase FTFSCW-IPM motor for electric vehicle application," *IEEE Trans. Veh. Technol.*, vol. 69, no. 1, pp. 282–292, Jan. 2020.

[19] B. C. Mecrow, A. G. Jack, J. A. Haylock, and J. Coles, "Fault-tolerant permanent magnet machine drives," *IEE Proc.-Electric Power Appl.*, vol. 143, no. 6, pp. 437–442, Nov. 1996.

[20] B. Wang, J. Wang, A. Griffo, and W. Hua, "Effective turn fault mitigation by creating zero sequence current path for a triple redundant 3-phase PMA SynRM," *IEEE Trans. Power Electron.*, vol. 34, no. 11, pp. 11080–11089, Nov. 2019.

[21] P. Arumugam, T. Hamiti, C. Brunson, and C. Gerada, "Analysis of vertical strip wound fault-tolerant permanent magnet synchronous machines," *IEEE Trans. Ind. Electron.*, vol. 61, no. 3, pp. 1158–1168, Mar. 2014.

[22] V. Nguyen et al., "A method for incipient interturn fault detection and severity estimation of induction motors under inherent asymmetry and voltage imbalance," *IEEE Trans. Transp. Electrific.*, vol. 3, no. 3, pp. 703–715, Sep. 2017.

[23] Y. Gritli, M. Mengoni, C. Rossi, A. Tani, D. Casadei, and G. Serra, "Experimental assessment of winding inter-turn short-circuits fault signatures in six-phase ac permanent magnet synchronous motors," *IET Renew. Power Gener.*, vol. 14, no. 15, pp. 2791–2800, Nov. 2020.

[24] S. Nandi and H. A. Toliyat, "Novel frequency-domain-based technique to detect stator interturn faults in induction machines using stator-induced voltages after switch-off," *IEEE Trans. Ind. Appl.*, vol. 38, no. 1, pp. 101–109, Jan./Feb. 2002.

[25] A. G. Yepes, J. Doval-Gandoy, F. Baneira, and H. A. Toliyat, "Speed estimation based on rotor slot harmonics in multiphase induction machines under open-phase fault," *IEEE Trans. Power Electron.*, vol. 33, no. 9, pp. 7980–7993, Sep. 2018.

[26] M. B. K. Bouzid and G. Champenois, "New expressions of symmetrical components of the induction motor under stator faults," *IEEE Trans. Ind. Electron.*, vol. 60, no. 9, pp. 4093–4102, Sep. 2013.

[27] M. Arkan, D. K. Perovic, and P. Unsworth, "Online stator fault diagnosis in induction motors," *IEE Proc.-Electric Power Appl.*, vol. 148, no. 6, pp. 537–547, Nov. 2001.

[28] P. Zhang, Y. Du, T. G. Habetler, and B. Lu, "A survey of condition monitoring and protection methods for medium-voltage induction motors," *IEEE Trans. Ind. Appl.*, vol. 47, no. 1, pp. 34–46, Jan./Feb. 2011.

[29] A. J. M. Cardoso, S. M. A. Cruz, and D. S. B. Fonseca, "Inter-turn stator winding fault diagnosis in three-phase induction motors, by Park's vector approach," *IEEE Trans. Energy Convers.*, vol. 14, no. 3, pp. 595–598, Sep. 1999.

[30] G. M. Joksimovic and J. Penman, "The detection of inter-turn short circuits in the stator windings of operating motors," *IEEE Trans. Ind. Electron.*, vol. 47, no. 5, pp. 1078–1084, Oct. 2000.

[31] S. Nandi, S. Ahmed, and H. A. Toliyat, "Detection of rotor slot and other eccentricity related harmonics in a three phase induction motor with different rotor cages," *IEEE Trans. Energy Convers.*, vol. 16, no. 3, pp. 253–260, Sep. 2001.

[32] S. Nandi, R. M. Bharadwaj, and H. A. Toliyat, "Performance analysis of a three-phase induction motor under mixed eccentricity condition," *IEEE Trans. Energy Convers.*, vol. 17, no. 3, pp. 392–399, Sep. 2002.

[33] E. Levi, "Multiphase electric machines for variable-speed applications," *IEEE Trans. Ind. Electron.*, vol. 55, no. 5, pp. 1893–1909, May 2008.

[34] M. Duran and F. Barrero, "Recent advances in the design, modeling and control of multiphase machines–Part 2," *IEEE Trans. Ind. Electron.*, vol. 63, no. 1, pp. 459–468, Jan. 2016.

[35] A. G. Yepes, O. Lopez, I. Gonzalez-Prieto, M. Duran, and J. Doval-Gandoy, "A comprehensive survey on fault tolerance in multiphase ac drives, Part 1: General overview considering multiple fault types," *Machines*, vol. 10, no. 3, 2022, Art. no. 208.

[36] A. G. Yepes, I. Gonzalez-Prieto, O. Lopez, M. Duran, and J. Doval-Gandoy, "A comprehensive survey on fault tolerance in multiphase ac drives, Part 2: Phase and switch open-circuit faults," *Machines*, vol. 10, no. 3, 2022, Art. no. 221.

[37] I. Gonzalez-Prieto, M. J. Duran, and F. J. Barrero, "Fault-tolerant control of six-phase induction motor drives with variable current injection," *IEEE Trans. Power Electron.*, vol. 32, no. 10, pp. 7894–7903, Oct. 2017.

[38] W. N. W. A. Munim, M. J. Duran, H. S. Che, M. Bermúdez, I. Gonzalez-Prieto, and N. A. Rahim, "A unified analysis of the fault tolerance capability in six-phase induction motor drives," *IEEE Trans. Power Electron.*, vol. 32, no. 10, pp. 7824–7836, Oct. 2017.

[39] F. Baneira, J. Doval-Gandoy, A. G. Yepes, O. Lopez, and D. Perez-Estevez, "Control strategy for multiphase drives with minimum losses in the full torque operation range under single open-phase fault," *IEEE Trans. Power Electron.*, vol. 32, no. 8, pp. 6275–6285, Aug. 2017.

[40] L. Alberti and N. Bianchi, "Experimental tests of dual three-phase induction motor under faulty operating condition," *IEEE Trans. Ind. Electron.*, vol. 59, no. 5, pp. 2041–2048, May 2012.

[41] A. Gonzalez-Prieto, I. Gonzalez-Prieto, A. G. Yepes, M. J. Duran, and J. Doval-Gandoy, "On the advantages of symmetrical over asymmetrical multiphase ac drives with even phase number using direct controllers," *IEEE Trans. Ind. Electron.*, vol. 69, no. 8, pp. 7639–7650, Aug. 2022.

[42] E. Pazouki, M. Z. Islam, S. S. R. Bonthu, and S. Choi, "Eccentricity fault detection in multiphase permanent magnet assisted synchronous reluctance motor," in *Proc. IEEE Int. Electric Mach. Drives Conf.*, 2015, pp. 240–246.

[43] C. López-Torres, J.-R. Riba, A. Garcia, and L. Romeral, "Detection of eccentricity faults in five-phase ferrite-PM assisted synchronous reluctance machines," *Appl. Sci.*, vol. 7, no. 6, May 2017, Art. no. 565.
[44] Y. Maouche, M. E. K. Oumaamar, A. L. Nemmour, and A. Khezzar, "Voltage signatures between two sub-windings in dual three-phase induction motor under static air-gap eccentricity," in *Proc. 8th Int. Conf. Elect. Electron. Eng.*, 2013, pp. 258–262.
[45] T. Wang, J. Huang, B. Lin, M. Kang, J. Chen, and W. Kong, "Eccentricity detection of a six-phase induction motor with HFI," *IET Electric Power Appl.*, vol. 13, no. 11, pp. 1717–1725, Mar. 2019.
[46] R. N. Andriamalala, H. Razik, G. Didier, F. M. Sargos, C. R. da Silva, and E. R. C. da Silva, "A model of dual stator winding induction machine in case of stator and rotor faults for diagnosis purpose," in *Proc. IEEE Ind. Appl. Conf. 41st IAS Annu. Meeting*, vol. 5, Oct. 2006, pp. 2340–2345.
[47] C. R. da Silva et al., "A new approach for inter-turn short-circuit detection in six-phase induction motor," in *Proc. IECON - 32nd Annu. Conf. IEEE Ind. Electron.*, 2006, pp. 4969–4974.
[48] D. Foito, J. Maia, V. F. Pires, and J. F. Martins, "Fault diagnosis in six-phase induction motor using a current trajectory mass center," *Measurement*, vol. 51, no. 1, pp. 164–173, May 2014.
[49] F. Immovilli, C. Bianchini, E. Lorenzani, A. Bellini, and E. Fornasiero, "Evaluation of combined reference frame transformation for interturn fault detection in permanent-magnet multiphase machines," *IEEE Trans. Ind. Electron.*, vol. 62, no. 3, pp. 1912–1920, Mar. 2015.
[50] V. M. Sundaram and H. A. Toliyat, "Stator inter-turn fault detection for seamless fault-tolerant operation of five-phase induction motors," in *Proc. IEEE Energy Convers. Congr. Expo.*, 2016, pp. 1–8.
[51] H. B. B. Abad, M. Ojaghi, and A. Taheri, "Extra freedom degrees of six-phase induction motors used to diagnose stator inter-turn faults," *Elect. Power Compon. Syst.*, vol. 49, no. 3, pp. 294–307, Feb. 2021.
[52] H. B. B. Abad, M. Ojaghi, and A. Taheri, "Efficient index for detecting the stator winding interturn fault in six-phase squirrel-cage induction motors," *Measurement*, vol. 184, Nov. 2021, Art. no. 109912.
[53] E. Amirouche, K. Iffouzar, A. Houari, K. Ghedamsi, and D. Aouzellag, "New diagnostic and severity estimation method for inter-turn short fault for dual star permanent magnet synchronous generator," *Arab J. Sci. Eng.*, vol. 47, no. 3, pp. 3573–3581, Jan. 2022.
[54] A. G. Yepes et al., "Selection criteria of multiphase induction machines for speed-sensorless drives based on rotor slot harmonics," *IEEE Trans. Ind. Electron.*, vol. 63, no. 8, pp. 4663–4673, Aug. 2016.
[55] R. M. Tallam, T. G. Habetler, and R. G. Harley, "Transient model for induction machines with stator winding turn faults," *IEEE Trans. Ind. Appl.*, vol. 38, no. 3, pp. 632–637, May/Jun. 2002.
[56] M. Jones, S. N. Vukosavic, D. Dujic, and E. Levi, "A synchronous current control scheme for multiphase induction motor drives," *IEEE Trans. Energy Convers.*, vol. 24, no. 4, pp. 860–868, 2009.
[57] A. G. Yepes, J. Malvar, A. Vidal, O. Lopez, and J. Doval-Gandoy, "Current harmonics compensation based on multiresonant control in synchronous frames for symmetrical n-phase machines," *IEEE Trans. Ind. Electron.*, vol. 62, no. 5, pp. 2708–2720, May 2015.
[58] A. G. Yepes, J. Doval-Gandoy, F. Baneira, D. Perez-Estevez, and O. Lopez, "Current harmonic compensation for n-phase machines with asymmetrical winding arrangement and different neutral configurations," *IEEE Trans. Ind. Appl.*, vol. 53, no. 6, pp. 5426–5439, Nov./Dec. 2017.
[59] A. Pantea et al., "Fault-tolerant control of a low-speed six-phase induction generator for wind turbines," *IEEE Trans. Ind. Appl.*, vol. 55, no. 1, pp. 426–436, Jan./Feb. 2019.
[60] M. Salehifar, R. S. Arashloo, J. M. Moreno-Equilaz, V. Sala, and L. Romeral, "Fault detection and fault tolerant operation of a five phase PM motor drive using adaptive model identification approach," *IEEE Trans. Emerg. Sel. Topics Power Electron.*, vol. 2, no. 2, pp. 212–223, Jun. 2014.
[61] O. Dieterle, T. Greiner, and P. Heidrich, "Control of a PMSM with quadruple three-phase star-connected windings under inverter short-circuit fault," *IEEE Trans. Ind. Electron.*, vol. 66, no. 1, pp. 685–695, Jan. 2019.
[62] J. A. Haylock, B. C. Mecrow, A. G. Jack, and D. J. Atkinson, "Operation of a fault tolerant PM drive for an aerospace fuel pump application," *IEE Proc.-Electric Power Appl.*, vol. 145, no. 5, pp. 441–448, Sep. 1998.
[63] V. Climente-Alarcon, J. Antonino-Daviu, A. Haavisto, and A. Arkkio, "Diagnosis of induction motors under varying speed operation by principal slot harmonic tracking," *IEEE Trans. Ind. Appl.*, vol. 51, no. 5, pp. 3591–3599, Sep./Oct. 2015.
[64] A. J. M. Cardoso, E. S. Saraiva, M. L. Sousa Mateus, and A. L. Ramalho, "On-line detection of airgap eccentricity in 3-phase induction motors, by Park's vector approach," in *Proc. IEE 5th Int. Conf. Elect. Mach. Drives*, 1991, pp. 61–66.
[65] A. G. Yepes and J. Doval-Gandoy, "Simple carrier-based PWM for prolonged high dc-link utilization for symmetrical and asymmetrical n-phase ac drives," *IEEE Trans. Power Electron.*, vol. 36, no. 8, pp. 8696–8712, Aug. 2021.
[66] A. G. Yepes, J. Doval-Gandoy, F. Baneira, and H. Toliyat, "Comparison of stator winding connections in multiphase drives under healthy operation and with one open converter leg," *IET Electric Power Appl.*, vol. 14, no. 4, pp. 584–596, Apr. 2020.
[67] M. J. Duran, I. Gonzalez-Prieto, M. Bermudez, F. Barrero, H. Guzman, and M. R. Arahal, "Optimal fault-tolerant control of six-phase induction motor drives with parallel converters," *IEEE Trans. Ind. Electron.*, vol. 63, no. 1, pp. 629–640, Jan. 2016.
[68] K. N. Gyftakis and J. C. Kappatou, "The zero-sequence current as a generalized diagnostic mean in Δ-connected three-phase induction motors," *IEEE Trans. Energy Convers.*, vol. 29, no. 1, pp. 138–148, Mar. 2014.
[69] A. S. Abdel-Khalik, R. A. Hamdy, A. M. Massoud, and S. Ahmed, "Post-fault control of scalar (V/F) controlled asymmetrical six-phase induction machines," *IEEE Access*, vol. 6, pp. 59211–59220, 2018.
[70] H. S. Che, E. Levi, M. Jones, W.-P. Hew, and N. A. Rahim, "Current control methods for an asymmetrical six-phase induction motor drive," *IEEE Trans. Power Electron.*, vol. 29, no. 1, pp. 407–417, Jan. 2014.

Alejandro G. Yepes (Senior Member, IEEE) received the M.Sc. and Ph.D. degrees in electrical engineering from Universidade de Vigo, Vigo, Spain, in 2009 and 2011, respectively.

Since 2008, he has been with the Applied Power Electronics Technology Research Group, Universidade de Vigo. From 2016 to 2018, he stayed with the Department of Electrical and Computer Engineering, Texas A&M University, College Station, TX, USA, after which he returned to Universidade de Vigo. His research interests are in the areas of ac power conversion, with special focus, currently, on multiphase drives.

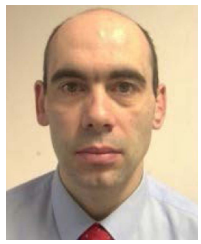

Davide S. B. Fonseca (Member, IEEE) was born in Castelo Branco, Portugal, on December 23, 1972. He received the Diploma in electrical engineering from the University of Coimbra, Coimbra, Portugal, in 1996 and the Ph.D. degree in electrical engineering from the University of Beirã Interior, Covilhã, Portugal, in 2008.

He has been with the University of Beira Interior, Covilha, Portugal, since 1997, where he is currently an Assistant Professor with the Department of Electromechanical Engineering and the Coordinator of the Electrical Machines and Power Electronics Laboratory. He is also Member of CISE – Electromechatronic Systems Research Centre. His research interests are focused on fault analysis and fault diagnostic in electrical drives.

Hugo R. P. Antunes was born in Lisbon, Portugal, on December 4, 1996. He received the B.Sc. and M.Sc. degrees in electric and computer engineering from the University of Beira Interior, Covilhã, Portugal, in 2018 and 2020, respectively. He is currently working toward the Ph.D. degree in electric and computer engineering with the University of Beira Interior, and CISE – Electromechatronic Systems Research Centre, Covilhã, Portugal.

His research interests are focused on condition monitoring, computational modelling, and fault diagnosis in multiphase induction machines.

Oscar López (Senior Member, IEEE) received the M.Sc. and Ph.D. degrees in electrical engineering from the University of Vigo, Vigo, Spain, in 2001 and 2009, respectively.

Since 2004, he has been an Assistant Professor with the University of Vigo. He is a member of the Applied Power Electronics Technology Research Group, University of Vigo. His research interests include the areas of ac power switching converters technology.

Antonio J. Marques Cardoso (Senior Member, IEEE) received the Dipl. Eng., Dr. Eng., and Habilitation degrees from the University of Coimbra, Coimbra, Portugal, in 1985, 1995 and 2008, respectively, all in electrical engineering.

From 1985 until 2011, he was with the University of Coimbra, where he was the Director of the Electrical Machines Laboratory. Since 2011, he has been with the University of Beira Interior (UBI), Covilhã, Portugal, where he is a Full Professor with the Department of Electromechanical Engineering and Director of CISE - Electromechatronic Systems Research Centre (http://cise.ubi.pt). He was a Vice-Rector of UBI from 2013 to 2014. His research interests are focused on fault diagnosis and fault tolerance of electrical machines, power electronics and drives. He is the author of a book entitled *Fault Diagnosis in Three-Phase Induction Motors* (Coimbra Editora, 1991, in Portuguese), editor of a book entitled *Diagnosis and Fault Tolerance of Electrical Machines, Power Electronics and Drives* (IET/SciTech, U.K., 2018), and also author of more than 500 papers published in technical journals and conference proceedings.

Dr. Cardoso currently serves as Editor-in-Chief for the MDPI journal *Machines*, and Associate Editor for the IEEE TRANSACTIONS ON INDUSTRY APPLICATIONS, IEEE TRANSACTIONS ON POWER ELECTRONICS, *IEEE Journal of Emerging and Selected Topics in Power Electronics*, *IEEE Open Journal of the Industrial Electronics Society*, as well of the Springer *International Journal of Systems Assurance Engineering and Management*.

Jesús Doval-Gandoy (Member, IEEE) received the M.Sc. and Ph.D. degrees in electrical engineering from the Polytechnic University of Madrid, Madrid, Spain, and from the Universidade de Vigo, Vigo, Spain, in 1991 and 1999, respectively.

He is currently a Professor and the Head of the Applied Power Electronics Technology Research Group (APET), Universidade de Vigo. His research interests are in the areas of ac power conversion.